Bulletin of the Seismological Society of America, Vol. 103, No. 1, pp. 595–600, February 2013, doi: 10.1785/0120120253

Ⓔ

Short Note

Tectonic Tremor beneath Cuba Triggered by the M_w 8.8 Maule and M_w 9.0 Tohoku-Oki Earthquakes

by Zhigang Peng, Hector Gonzalez-Huizar, Kevin Chao, Chastity Aiken, Bladimir Moreno, and Gregory Armstrong

Abstract We provide additional evidence of tectonic tremor in Cuba triggered by the 2010 M_w 8.8 Maule, Chile, and the 2011 M_w 9.0 Tohoku-Oki, Japan, earthquakes. The high-frequency tremor signals are modulated by long-period surface waves, similar to triggered tremors observed in other tectonically active regions. We are able to locate two tremor sources triggered by the Tohoku-Oki earthquake near the east–west trending Oriente fault around Guantanamo Bay. The tremor around Guantanamo Bay was triggered primarily by a Love wave of the Maule mainshock, and by both Love and Rayleigh waves of the Tohoku-Oki mainshock. This is consistent with frictional failures at a vertical strike-slip fault under a Coulomb failure criterion.

Online Material: Figure of envelope functions of tremor records, and movies of spectogram and tremor correlation.

Introduction

Deep tectonic tremor is a recently discovered seismic phenomenon (Peng and Gomberg, 2010; Beroza and Ide, 2011; and references therein). It is recorded as a non-impulsive, low-amplitude, and long-duration signal, and is often accompanied by slow-slip events. Tremor is extremely stress sensitive, and can be triggered instantaneously by passing surface waves of regional and teleseismic earthquakes (e.g., Peng and Gomberg, 2010). Previously, tremor has been primarily observed along major subduction zones around the Pacific Rim (Beroza and Ide, 2011). Recently, tremor is being identified at diverse tectonic environments. These include the Central Range in Taiwan (Chao, Peng, Wu, *et al.*, 2012), which is an arc-continent collision environment; the strike-slip San Andreas Fault system in California (Shelly and Harkdebeck, 2010; Chao, Peng, Fabian, *et al.*, 2012); the Queen Charlotte Fault, a transform fault off the coast of western Canada that separates the North American and Pacific plates (Aiken *et al.*, 2012); and the Alpine fault in New Zealand (Wech *et al.*, 2012), a transpressional structure that accommodates relative motions between the Australian and Pacific plates.

Recently, Gonzalez-Huizar *et al.* (2012) analyzed the recordings from a seismic station near Guantanamo Bay, Cuba, and found tremor triggered by the 2010 M_w 8.8 Maule, Chile, and 2011 M_w 9.0 Tohoku-Oki, Japan, earthquakes. The corresponding epicentral distances to Guantanamo Bay are 6208 and 12,471 km, respectively. Based on clear high-frequency tremor signals modulated by the Love wave, they suggested that tremor occurred on the nearby left-lateral Oriente fault (OF), which accommodates transpressive deformation between the North American and Caribbean plates. However, with a single-station recording they were unable to accurately locate the source of triggered tremor. The focus of this study, then, is to provide additional evidence of triggered tremor beneath Cuba. We analyze and locate the sources of the triggered tremor using the seismic data recorded by the local Cuba Seismograph Network (CSN). In addition, we estimate the triggering potentials of the teleseismic surface waves and compare them with the tremor observations to better understand the physical mechanisms of tremor triggering.

Data and Analysis Procedure

The seismic data analyzed in this study were recorded by the broadband station GTBY near Guantanamo Bay, which belongs to the USGS Caribbean seismic network CU, and by 11 stations (6 broadband and 5 short-period) in the CSN (Moreno, 2002). The CSN started continuous recording in 2011. Nine stations in the CSN recorded the 2011 Tohoku-Oki earthquake, so in total we have ten stations for further study (Fig. 1). In addition, we also analyze the seismic data recorded during the 2010 M_w 8.8 Maule mainshock by the single station GTBY.

The analysis procedure generally follows our previous studies (e.g., Chao, Peng, Gonzalez-Huizar, *et al.*, 2012) and is briefly described here. First, we apply a 2–16 Hz

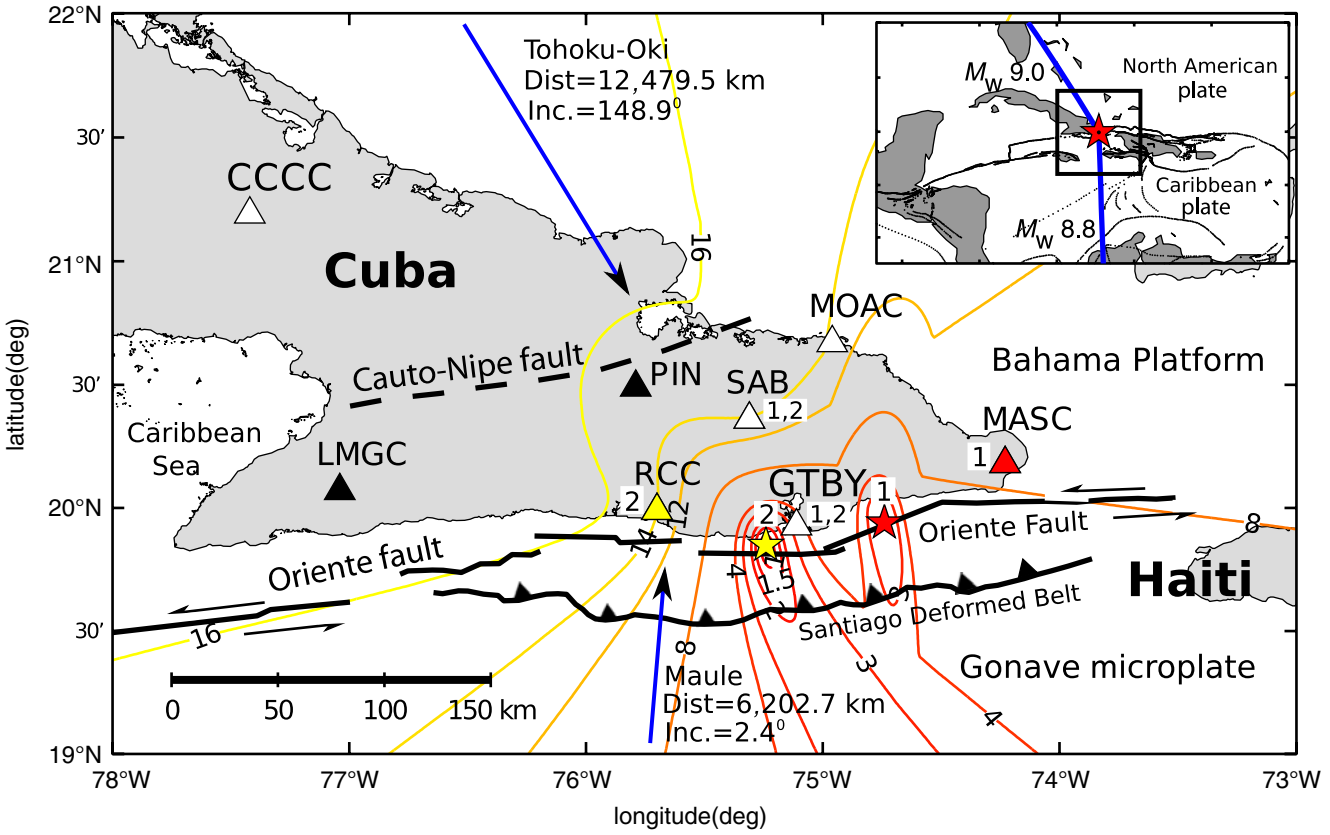

Figure 1. The study region in Cuba. The stars mark the two tremor locations triggered during the surface waves of the 2011 M_w 9.0 Tohoku-Oki mainshock. The solid and dashed lines denote the Oriente fault (OF) and the Cauto-Nipe fault (CNF). The contour lines denote the root mean square (rms) differences (in seconds) between the observed and predicted *S*-wave travel times of tremor bursts. The two stars mark the best-fitting locations for tremor sources 1 and 2, respectively. The triangles mark the seismic stations analyzed in this study, with numbers denoting different observations of signals from the two tremor sources: stations GTBY and SAC, 1,2; station MASC: 1; station RCC: 2. The black triangles mark stations LMGC and PIN that recorded triggered tremor possibly from the CNF. The arrow marks the back-azimuth of the incoming surface waves from the 2010 M_w 8.8 Maule and 2011 M 9.0 Tohoku-Oki mainshocks. The inset shows the great circle path between the mainshocks and the study region. The color version of this figure is available only in the electronic edition.

band-pass or 5 Hz high-pass filter to the seismic data, and compare the high-frequency signals with instrument-correlated broadband seismograms recorded at each station. We identify triggered tremor as high-frequency, non-impulsive signals that are in phase with the large-amplitude teleseismic waves. In addition, we convert the seismic data into sounds and animations (Kilb *et al.*, 2012) and use them to illustrate and assist in the identification of triggered tremor.

Next, we compute the envelope functions from the three-component, high-pass-filtered seismograms, smooth them by applying a 10-s low-pass filter, decimate to 1 sample/s, and stack them to obtain a single envelope function for each station. Then we verify whether the high-frequency tremor signals are coherent at nearby stations. If so, we manually identify the peak of each tremor burst. Next, we compute the differential travel times via envelope cross correlations at nearby stations (Chao, Peng, Gonzalez-Huizar, *et al.*, 2012), and perform a grid search (with a step of 0.01°) to find the best-fitting tremor location that matches the observed differential travel times with the predicted ones using a 1D *S*-wave velocity model of the region (Moreno *et al.*, 2002). Given that the technique does not provide good constraints in the tremor vertical location, we fix the tremor depth to be 20 km. This is the average Moho depth in this region (Moreno *et al.*, 2002), and is close to the tremor depth observed in similar tectonic environments, such as along the San Andreas Fault (Shelly and Hardebeck, 2010).

General Observations

Out of the ten stations we have examined, six have recorded tremor-like signals during the passing surface waves of the 2011 Tohoku-Oki mainshock (Fig. 1). Figure 2 shows an example recorded at station CU.GTBY. Some weak tremor occurred during the long-period (~100 s) Love waves between 2700 and 3100 s, followed by stronger tremor bursts during the subsequent short-period Love waves (~20 s) and Rayleigh waves. Figure 3 shows similar observations at station CU.GTBY during the 2010 Maule mainshock. Strong tremor was initiated by the large-amplitude Love waves, and continued during and after the subsequent Rayleigh waves.

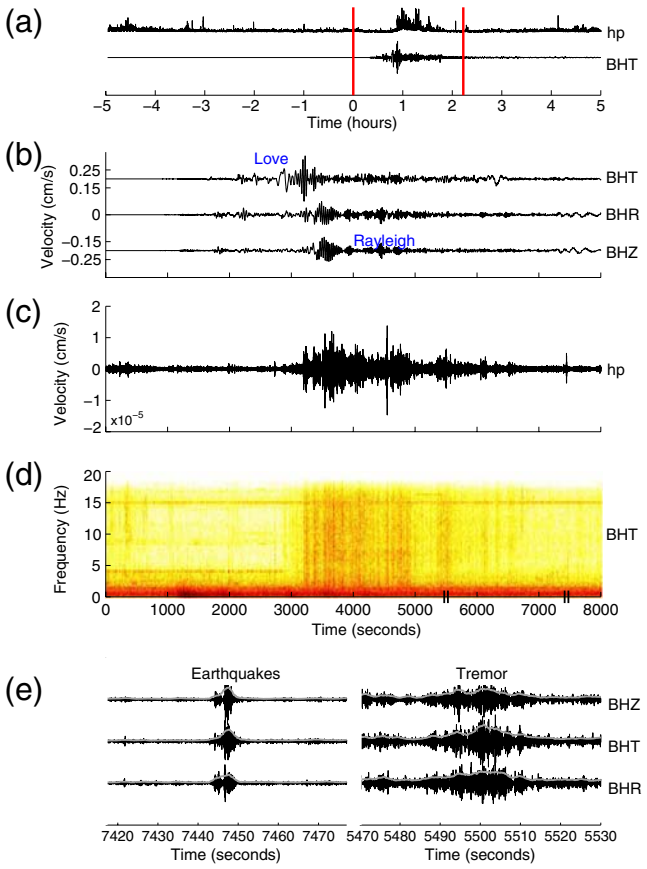

Figure 2. Triggered tremor in Cuba recorded at station CU.GTBY during the 2011 M_w 9.0 Tohoku-Oki earthquake that occurred ~12,471 km away. (a) A comparison between the broadband (BH) and 5-Hz high-pass filtered (hp) data for the transverse component (T) 5 h before and after the Tohoku-Oki mainshock. The two vertical lines mark the time window around the teleseismic waves of the Tohoku-Oki mainshock. (b) The broadband three-component (BHT: transverse; BHR: radial; BHZ: vertical) velocity seismograms showing the teleseismic waves of the Tohoku-Oki mainshock. (c) A zoom-in plot of the 5-Hz high-pass filtered data at BHT component showing triggered tremor. (d) The corresponding spectrogram. (e) A zoom-in plot showing the high-frequency signals from a local earthquake. The gray lines correspond to the smoothed envelope function. (f) A zoom-in plot showing the tremor signals during the Rayleigh waves. The corresponding animation is shown in Ⓔ movie S1 in the electronic supplement. The color version of this figure is available only in the electronic edition.

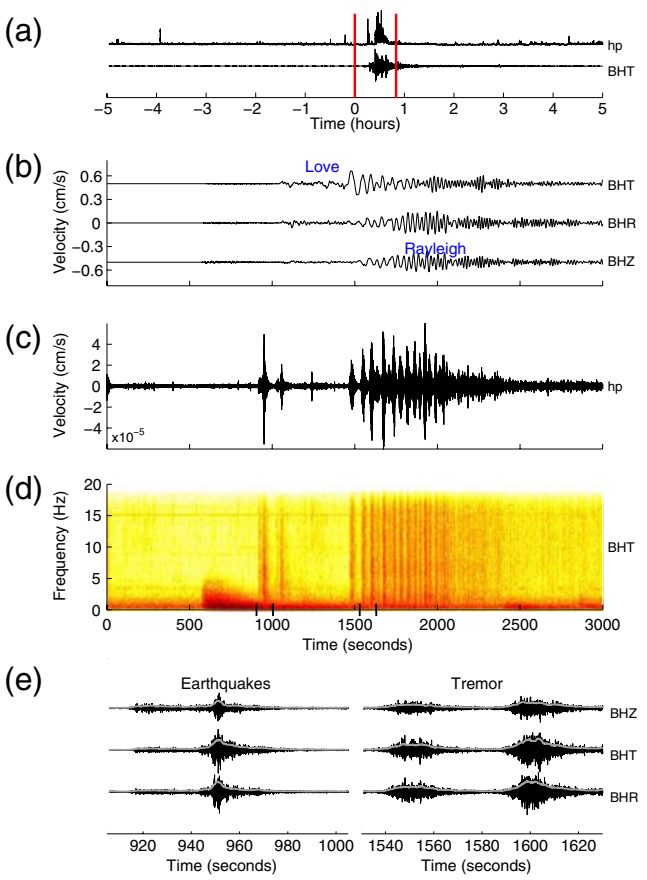

Figure 3. Triggered tremor in Cuba recorded at station CU.GTBY during the 2010 M_w 8.8 Maule earthquake that occurred ~6208 km away. Other symbols and notations are the same as in Figure 2. The corresponding animation is shown in Ⓔ movie S2 in the electronic supplement. The color version of this figure is available only in the electronic edition.

The amplitudes of the high-frequency signals during the teleseismic waves are larger than those at other times either before or after the mainshocks (Figs. 2 and 3), suggesting that they are triggered by the surface waves.

The corresponding animations, with sounds, are shown in Ⓔ movies S1 and S2 in the electronic supplement to this article. The teleseismic *P* waves sound like distant thunders, while local and regional earthquake signals generally sound like gunshots or firecrackers, probably because of their short durations and abundance in high frequencies. In comparison, triggered tremor signals sound more like rattlesnakes or the start of a steam engine, due to their extended durations and relative deficiency in high frequencies.

Next, we separate the observations during the 2011 Tohoku-Oki mainshock into four groups based on visual examination of their waveform coherences (Fig. 4). The first group includes stations GTBY, MASC, and SAB, which recorded the coherent signals for the first six tremor bursts during the short-period Love waves (see Ⓔ Fig. S1 in the electronic supplement). Although similar tremor signals are recorded at station RCC, it is relatively difficult to isolate different bursts, so we do not include the waveform from this station to locate tremor. Using the first three stations with higher similarities, we find the best-fitting tremor location to be $-74.74° \pm 0.11°$, and $19.94° \pm 0.13°$, ~39 km east of station GTBY. The second group of tremor signals is best recorded at stations GTBY, SAB, and RCC during the short-period Rayleigh waves. Again, although we could track similar tremor signals at station MASC, they are not as clean as those at the other three stations, suggesting that the source is further from station MASC (Ⓔ see Fig. S1 in the supplement). The best-fitting tremor location is $-75.24° \pm 0.03°$ and $19.85° \pm 0.07°$, ~16 km southwest of station GTBY. In both cases, the uncertainties in the latitudes are slightly larger

than in the longitudes, mostly due to the one-sided station distributions. In viewing the location uncertainties, we suggest that the tremor occurred on or close to the east–west trending OF (Fig. 1).

The third tremor source was best recorded at station LMGC in Las Mercedes (Fig. 4). The tremor was initiated by the Love wave starting at ~2850 s. The subsequent tremor was also clearly modulated by the Love wave. Interestingly, the large-amplitude Rayleigh waves between 3400 and 3800 s only triggered weak tremor. Additional tremor-like signals occurred between 3900 and 4500 s after the passing of large-amplitude surface waves. Because such signals were only recorded at station LMGC, we could not determine their locations. However, because this station is about 50 km south of the east-northeast–west-southwest trending Cauto Nipe Fault (CNF), it is very likely that the tremor occurred on or near the CNF (Fig. 1).

The fourth possible tremor was recorded at station PIN further inland, near Pinares (Fig. 4). Tremor occurred starting at ~3000 s immediately after the long-period Love wave, and additional tremor with larger amplitudes was modulated by the subsequent shorter-period Love wave. Some weak tremor occurred during the large-amplitude Rayleigh waves. Again, we assume that the tremor originates on or near the CNF due to its proximity to station PIN.

Dynamic Stress Modeling

In this section, we model the dynamic triggering of observed tremor using a simple Coulomb failure criterion. The detailed procedure generally follows that of previous studies (Gonzalez-Huizar and Velasco, 2011; Chao, Peng, Gonzalez-Huizar, *et al.*, 2012; Hill, 2012). We assume that tremor is produced by frictional failures at nearby major plate-boundary faults. We calculate the triggering potential as the Coulomb stress change, generated by the passing of the surface waves, on a vertical left-lateral strike-slip fault at 20 km depth. We use the same elastic parameters defined in Hill (2012) for single-frequency (20 s), equal-amplitude Love and Rayleigh waves, to calculate their triggering potential as function of incident angles (Fig. 5). Surface waves from the Tohoku-Oki earthquake have near −58° incidence (back azimuth of 328°) on the east–west trending OF in Cuba. In this case, the Rayleigh wave has higher triggering potential than the Love wave, which is generally consistent with the predominant Rayleigh triggering observed at CU.GTBY and other nearby stations (Figs. 2 and 4). In comparison, surface waves from the Maule mainshock have near strike-normal incidence on the OF, which would result in maximum Love-wave triggering potential. This is consistent with the observations of predominant Love-wave triggering during the Maule mainshock, although tremor continued during the subsequent Rayleigh waves (Fig. 3). Finally, the teleseismic wave from the Tohoku-Oki mainshock also has a near strike-normal incidence (~80°) on the CNF. If we assume that the tremor observed at stations LMGC and PIN were generated from the CNF, then we would expect to see higher triggering potential for the Love wave. Again, this is qualitatively consistent with the predominant Love-wave-triggered tremor observed at these stations.

In addition to the simple modeling of triggering potential, we also compute the dynamic stress waves (stressgrams) and compare them with the tremor observations. The procedure for computing the stress grams follows that in Chao, Peng, Gonzalez-Huizar, *et al.* (2012) and is briefly

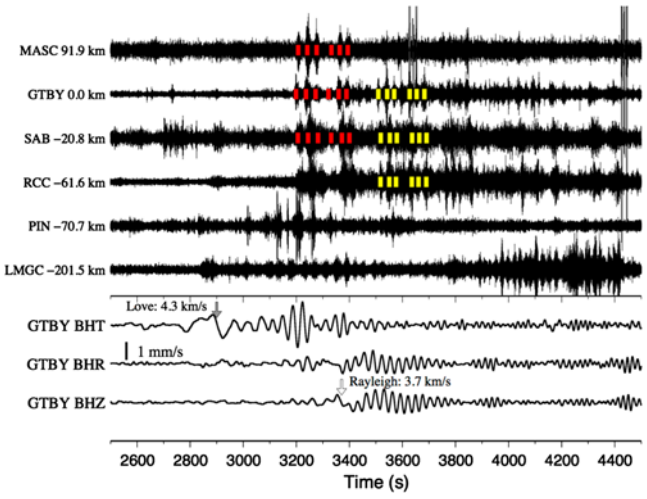

Figure 4. The 2–16 Hz band-pass filtered seismograms in the north component showing the moveout of triggered tremor at multiple source regions in Cuba. The station names and distances to station GTBY are marked to the left of the seismograms. The tremor bursts used to locate the tremor sources are marked with vertical dotted lines. The bottom three traces show the instrument-corrected seismograms in radial (BHR), vertical (BHZ), and transverse (BHT) components at station GTBY. The thick vertical bar marks the amplitude scale of surface waves. The color version of this figure is available only in the electronic edition.

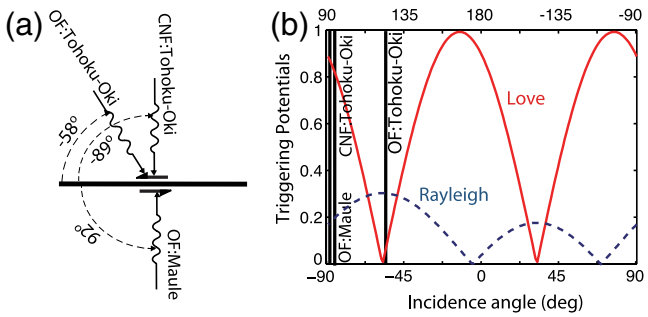

Figure 5. Surface-waves triggering potentials. (a) A simple schematic diagram for a strike-slip fault where arrows represent the incident angles of the teleseismic waves. (b) Love (solid) and Rayleigh (dashed) wave relative potentials to trigger tremor at 20-km depth on a vertical, left-lateral strike-slip fault with a coefficient of friction of 0.2. Vertical lines in triggering potential plots define the incident angle for each region where tremor was triggered. Multiplying the triggering potentials by the normalizing factor of 18.5 kPa gives the potentials in terms of Coulomb stress. The color version of this figure is available only in the electronic edition.

described here. We first measure the triggering wave's amplitudes and frequencies from consecutive peaks in the displacement seismograms. Next, we compute the dynamic stress tensors for those peak values and interpolate them to obtain time-dependent stress values. Because the tremor triggered during the Love and Rayleigh waves originated from slightly different locations, we compute the stress grams separately. We also take a smoothed envelope function of the tremor signals at station GTBY, time shift it back to the tremor source region, and compute the cross correlations with the stress grams for the Love and Rayleigh waves and the total stress values.

Figure 6 shows that the dynamic stresses from the short-period Love waves associated with the 2011 Tohoku-Oki earthquake match well with the first 6–7 bursts of tremor at 3150–3450 s with a correlation coefficient of 0.82, and the peak dynamic stress is on the order of 10 kPa. In comparison, the dynamic stresses from the Rayleigh waves are less than 5 KPa, and do not correlate with the tremor envelope. The later tremor at 3400–3700 s appears to correlate with the dynamic stresses from the Rayleigh waves, although the correlation value of 0.51 is not as high as during the Love waves.

Discussion

In this study, we provided additional evidence of tremor in Cuba triggered by large teleseismic earthquakes. Based on similar tremor waveforms recorded at the CSN and station CU.GTBY, we located two tremor sources that are close to the east–west trending OF. Although we were unable to determine their depths, given their non-impulsive waveforms, relative low-frequency contents, and clear modulations by the teleseismic surface waves, we inferred that the observed signals were most likely produced by deep tremor, consistent with those observed at other tectonically active regions (Peng and Gomberg, 2010). Similar features were observed for the tremor recorded by stations LMGC and PIN. However, we were unable to provide accurate locations, because they were not recorded at nearby stations. We inferred that they occurred on nearby CNF, although they could have originated from other similar faults in the study region.

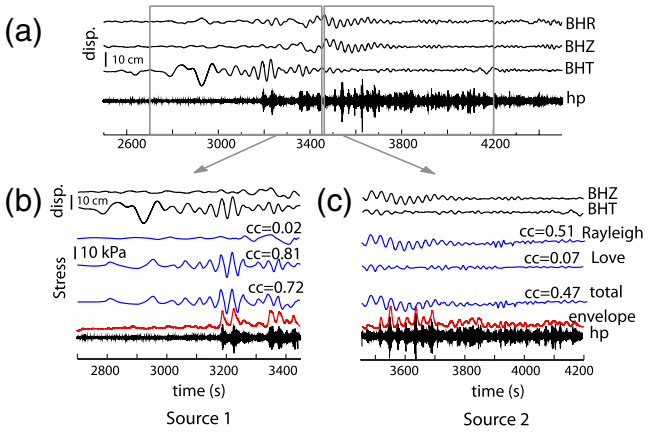

Figure 6. Time-dependent dynamic stress (stress grams) as a measurement of the potential of surface waves from the Tohoku-Oki earthquake to trigger tremor in Cuba. (a) Radial, vertical, and transverse displacement components recorded at station CU.GTBY. The two boxes mark the time window showing in panels (b) and (c). (b) Dynamic stresses caused by Love, Rayleigh, and combined (total) ground displacement for the first group of tremor source. The bottom panel is the high-pass-filtered seismogram and envelope showing the triggered tremor signals. The cross correlation (cc) between dynamic stress and triggered tremor's envelope is shown. All signals have been time shifted back to the triggered tremor source location. (c) Same as (b) for the second group of tremor source during the Rayleigh waves. The color version of this figure is available only in the electronic edition.

The tremor observed in this study was primarily triggered by the Love wave of the 2010 Maule earthquake, and by both Love and Rayleigh waves of the 2011 Tohoku-Oki earthquake. This is qualitatively consistent with the simple triggering potential for surface waves (Fig. 5), and is further confirmed by the stress grams shown in Figure 6 for the Tohoku-Oki event. We note that the calculated triggering potential shown in Figure 5 assumes equal amplitude for both Love and Rayleigh waves, and a constant period of 20 s. In reality, the amplitudes and periods of the surface waves changed with time. A better way to evaluate the triggering relationship is to perform a stress-gram analysis as done in Figure 6. However, because we do not have the CSN recording for the Maule earthquake, we cannot accurately locate the tremor triggered by this event. Hence, we have to rely on the simple calculation of the triggering potential as shown in Figure 5 to explain the observation for the Maule event.

As mentioned before, the OF is a left-lateral fault forming the boundary between the Caribbean plate (or the Gonave microplate) and the North American plate (Fig. 1). In addition to the left-lateral strike-slip motions, additional compressional deformation is accommodated by the Santiago deformed belt (Fig. 1), a 10–30-km-wide and 300-km-long narrow zone parallel to the OF (Calais *et al.*, 1998). The majority of the seismicity observed along the southern Cuban margin has occurred within this zone (Moreno *et al.*, 2002). Our two tremor locations (Fig. 1) are also close to the majority of the seismicity in this region.

So far tremor has been mostly observed along major plate-boundary faults that have relatively fast deformation rates (e.g., 1 cm/yr). However, because tremor is not observed everywhere along major faults, this is only a necessary, but not sufficient, condition. Peng and Gomberg (2010) suggested that other ambient conditions, such as existence of elevated fluid pressures at depth, or rock types, could also be important in tremor generation. Finally, triggered tremors are mostly found in places where ambient tremors have been identified, suggesting that triggered and ambient tremors are generated by similar failure processes, but with different loading conditions (Shelly *et al.*, 2011; Chao, Peng, Wu, *et al.*, 2012). That is, triggered tremor is driven by transient

dynamic stresses from teleseismic waves, while ambient tremor is loaded by local creep events or other unknown forces. Hence, we infer that ambient tremor could also occur around the OF in Cuba. Further geophysical studies of the velocity structures in this region, along with detailed search for triggered and ambient tremor, are needed to better understand the physical conditions for tremor generation and its relationship to background seismicity and large earthquakes in this region.

Data and Resources

Seismic data recorded by station CU.GTBY were downloaded from the IRIS Data Management Center (DMC) website (http://www.iris.edu/mda/CU/GTBY, last accessed August 2012) and are openly available. The seismic data recorded by the Cuba Seismic Network (CSN) are not open to public at this time (http://www.cenais.cu, last accessed August 2012).

Acknowledgments

We thank the IRIS DMC for achieving and distributing the seismic data recorded at station CU.GTBY. The manuscript benefits from useful comments by David Hill and an anonymous reviewer. Z. P., K. C., and G. A. are supported by National Science Foundation (NSF) CAREER Grant EAR-0956051 and its REU supplement, and H. G.-H. is supported by NSF Grant EAR-1053355. This material is based upon work supported by the National Science Foundation Graduate Research Fellowship for C. A. under NSF Grant DGE-1148903.

References

Aiken, C., Z. Peng, and K. Chao (2012). Triggered tremor along the Queen Charlotte Fault (abstract S33B-2551), 2012 Fall Meeting, *AGU*, San Francisco, California, S33B-2551.

Beroza, G. C., and S. Ide (2011). Slow earthquakes and nonvolcanic tremor, *Annu. Rev. Earth Planet. Sci.* **39,** 271–296, doi: 10.1146/annurev-earth-040809-152531.

Calais, E., J. Perrot, and B. Mercier de Lépinay (1998). Strike-slip tectonics and seismicity along the Northern Caribbean plate boundary from Cuba to Hispaniola, J. F. Dolan and P. Mann (Editors), Geol. Soc. Am. Special Paper, Vol. 326, 125–142.

Chao, K., Z. Peng, A. Fabian, and L. Ojha (2012). Comparisons of triggered tremor in California, *Bull. Seismol. Soc. Am.* **102,** no. 2, 900–908, doi: 10.1785/0120110151.

Chao, K., Z. Peng, H. Gonzalez-Huizar, C. Aiken, B. Enescu, H. Kao, A. A. Velasco, K. Obara, and T. Matsuzawa (2012). Global search of triggered tremor following the 2011 M_w 9.0 Tohoku-Oki earthquake, *Bull. Seismol. Soc. Am.*, **103**, no. 2B (in press).

Chao, K., Z. Peng, C. Wu, C.-C. Tang, and C.-H. Lin (2012). Remote triggering of non-volcanic tremor around Taiwan, *Geophys. J. Int.* **188,** 301–324, doi: 10.1111/j.1365-246X.2011.05261.x.

Gonzalez-Huizar, H., and A. A. Velasco (2011). Dynamic triggering: Stress modeling and a case study, *J. Geophys. Res.* **116,** B02304, doi: 10.1029/2009JB007000.

Gonzalez-Huizar, H., A. A. Velasco, Z. Peng, and R. Castro (2012). Remote triggered seismicity caused by the 2011, *M* 9.0 Tohoku-Oki, Japan earthquake, *Geophys. Res. Lett.* **39,** L10302, doi: 10.1029/2012GL051015.

Hill, D. P. (2012). Surface-wave potential for triggering tectonic (nonvolcanic) tremor–corrected, *Bull. Seismol. Soc. Am.* **102,** no. 6, 2337–2355.

Kilb, D., Z. Peng, D. Simpson, A. Michael, M. Fisher, and D. Rohrlick (2012). Listen, watch, learn: SeisSound video products, *Seismol. Res. Lett.* **83,** no. 2, 281–286, doi: 10.1785/gssrl.83.2.281.

Moreno, B. (2002), The new Cuban seismograph network, *Seismol. Res. Lett.* **73,** 505–518.

Moreno, B., M. Grandison, and K. Atakan (2002). Crustal velocity model along the southern Cuban margin: Implications for the tectonic regime at an active plate boundary, *Geophys. J. Int.* **151,** 632–645.

Peng, Z., and J. Gomberg (2010). An integrated perspective of the continuum between earthquakes and slow-slip phenomena, *Nature Geosci.* **3,** 599–607, doi: 10.1038/ngeo940.

Shelly, D. R., and J. L. Hardebeck (2010). Precise tremor source locations and amplitude variations along the lower-crustal central San Andreas Fault, *Geophys. Res. Lett.* **37,** L14301, doi: 10.1029/2010GL043672.

Shelly, D. R., Z. Peng, D. P. Hill, and C. Aiken (2011). Triggered creep as a possible mechanism for delayed dynamic triggering of tremor and earthquakes, *Nature Geosci.* **4,** 384–388.

Wech, A. G., C. M. Boese, T. A. Stern, and J. Townend (2012). Tectonic tremor and deep slow slip on the Alpine Fault, *Geophys. Res. Lett.* **39,** L10303, doi: 10.1029/2012GL051751.

School of Earth and Atmospheric Sciences
Georgia Institute of Technology
Atlanta, Georgia 30332
zpeng@gatech.edu
(Z.P., C.A.)

Geological Sciences
University of Texas at El Paso
El Paso, Texas 79902
(H.G.-H.)

Earthquake Research Institute
The University of Tokyo
Bunkyo-ku, Tokyo, Japan
(K.C.)

Centro Nacional Investigaciones Sismologicas
Santiago de Cuba
Cuba 90400
(B.M.)

Department of Geosciences
Georgia State University
Atlanta, Georgia 30303
(G.A.)

Manuscript received 9 August 2012